

Artificial Pupil Dilation for Data Augmentation in Iris Semantic Segmentation

Daniel P. Benalcazar

R&D Center SR-226

TOC Biometrics

Santiago, Chile

daniel.benalcazar@tocbiometrics.com

David A. Benalcazar

Pontificia Universidad

Catolica del Ecuador

Quito, Ecuador

dbenalcazar234@puce.edu.ec

Andres Valenzuela

R&D Center SR-226

TOC Biometrics

Santiago, Chile

andres.valenzuela@tocbiometrics.com

Abstract—Biometrics is the science of identifying an individual based on their intrinsic anatomical or behavioural characteristics, such as fingerprints, face, iris, gait, and voice. Iris recognition is one of the most successful methods because it exploits the rich texture of the human iris, which is unique even for twins and does not degrade with age. Modern approaches to iris recognition utilize deep learning to segment the valid portion of the iris from the rest of the eye, so it can then be encoded, stored and compared. This paper aims to improve the accuracy of iris semantic segmentation systems by introducing a novel data augmentation technique. Our method can transform an iris image with a certain dilation level into any desired dilation level, thus augmenting the variability and number of training examples from a small dataset. The proposed method is fast and does not require training. The results indicate that our data augmentation method can improve segmentation accuracy up to 15% for images with high pupil dilation, which creates a more reliable iris recognition pipeline, even under extreme dilation.

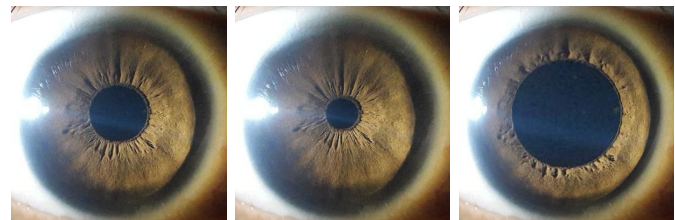
Keywords—iris recognition, semantic segmentation, data augmentation, pupil dilation.

I. INTRODUCTION

In modern times, it is ever more frequent to use biometric systems daily from unlocking smartphones to border controls. Those systems rely on the distinctive features of each individual, such as the shape of their face, the patterns of fingerprints, veins and iris tissue, and even the micro-expressions when one talks or walks [1]. Iris recognition in particular analyzes the pattern of the human iris that is made out of both changes in melanin coloration and structural folds that occur when this tissue changes the aperture of the pupil [2], [3]. The advantages of using the iris as a biometric pattern are that there is a high variability between individuals, the iris is protected by the cornea so it is unlikely to degrade over time, and it is a non-contactive, non-invasive and non-intrusive method [4], [5]. That is why India, for example, is using iris, along with fingerprints, for its Aadhaar national identification system of more than a billion individuals [6].

Our method, illustrated in Fig. 1, aims to improve robustness in iris segmentation. The process of Iris recognition, shown in Fig. 2, relies on the following steps. Iris segmentation, where the binary mask that encompasses the pixels of the iris is found

This research work has been partially funded by the TOC Biometrics R&D center SR-226 and SOVOS.



(a) Original image (b) Reduced dilation (c) Increased dilation

Fig. 1. Example of artificial dilation change. a) Original input image, dilation level $\lambda = R_{pupil}/R_{iris} = 0.282$. b) Artificially decreased dilation $\lambda = 0.150$. c) Artificially increased dilation $\lambda = 0.550$.

(Fig. 2b) [4]. Iris localization, in which the coordinates of the circles or ellipses that best fit the pupil and iris are computed (Fig. 2c) [5]. Normalization, where the annular iris surface is turned into a rectangle known as the Rubber Sheet (Fig. 2d) [4]. Encoding, where the information of the iris surface is encoded in a compact feature vector, which in some cases is binary [5]. Finally, comparison, where the encodings of two irises are compared to find if they belong to the same subject or not. This step can also compare one iris against a dataset to determine the identity of the subject [5].

In this research work, we focus on improving the first link of the chain, the segmentation stage, by making it robust for a wide range of pupil dilations. The dilation level λ is defined as the ratio between the pupil radius and the iris radius [7]. Traditional iris datasets were captured under controlled illumination environments, and small dilation variation [5]. However, studies have shown that images with extreme pupil dilation, in which the pupil is either too narrow or too large, can degrade iris recognition performance [7]–[9]. Those extreme cases are not uncommon since the iris can dilate because of illumination changes, as well as alcohol and drug consumption [8], [9]. Therefore, it is essential to obtain datasets with representative cases of those examples for modern deep-learning algorithms to generalize and produce good segmentation results at any dilation level [10].

That is why we propose a Data-Augmentation (DA) algorithm that artificially changes the dilation of input iris images, as seen in Fig. 1. In this way, the segmentation

network’s training process benefits from a wider variety of dilated images. This technique, in turn, makes the network more robust to extreme dilation conditions, as in the case of alcohol consumption [10]. We expect our method to increase the segmentation accuracy of any segmentation network, so we trained and tested seven of the most commonly used segmentation networks with and without our technique and compared the results.

As for the contributions of this work, we produced:

- An open-source DA function that artificially dilates the pupil in segmentation masks and iris images captured under Visible Light (VL) and Near Infrared Range (NIR) illumination.
- A fast DA method that increases iris segmentation performance in extremely dilated images, without requiring a training process.
- A benchmarking evaluation, showing the improvement in segmentation performances on state-of-the-art networks, as well as its the T-test significance.

II. RELATED METHODS

Original Iris Recognition methods relied on deterministic image processing techniques [2], [5], [6]. However, in recent years deep-learning methods have obtained a better performance since they can generalize well for wider populations and less restricted environments [10]–[18]. Some do not require training in the recognition stage [13], [19], and others even make use of the 3D structure of the iris tissue [20], [21].

A problematic facing all those methods is the need for extensive labeled datasets to train the segmentation network, [10], [16], [17]. Most available massive datasets, such as CASIA, UBIRIS and Notre Dame, were captured under controlled illumination conditions and specific capture devices [22]. On the other hand, newer, more challenging datasets are captured in the wild under a huge variety of conditions; however, they either contain fewer images or are not publicly available [10], [22]. The greater the number of examples with more variability, the better deep-learning methods can perform in real-world situations [10], [16], [23].

Hollingsworth et. al [7], and Arora et. al [8] studied how less restricted illumination conditions, as well as alcohol consumption, during image capture would detriment recognition performance. This is because, in extreme dilation conditions, the iris is more difficult to segment and the available iris area is too small to extract the biometric pattern successfully [7], [8]. Some research works have studied mathematical models for pupil dilation in order to mitigate this issue [9], [24], while Tapia et. al [10] captured an extensive dataset of irises in normal conditions, as well as under the influence of alcohol in order to train better segmentation networks capable of operating even under extreme dilation or constrictions.

An alternative to manually capturing and pre-processing a large dataset is to apply DA techniques on a small sample to increase the richness of the data artificially. Most common DA techniques include image translation, rotation, flipping, affine transformations, brightness and contrast adjustment, color

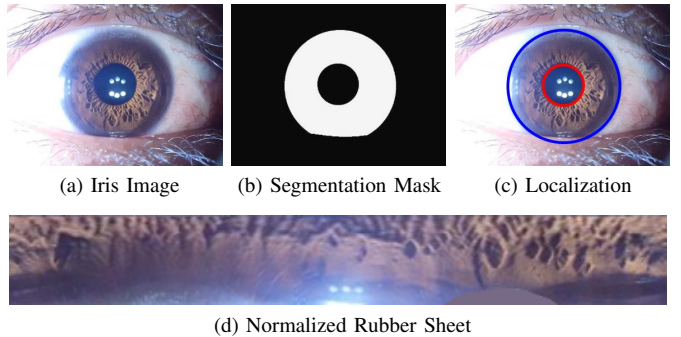


Fig. 2. Iris segmentation and normalization. a) Input image. b) Segmentation mask produced by deep-learning methods. c) Iris and pupil localization. d) Normalized iris image, known as rubber sheet.

shifting, and noise addition [10]. Most recently, Generative Adversarial Networks (GAN) have been used to artificially generate new iris images of nonexistent subjects, thus increasing the number of examples and enhancing performance [25]–[28]. However, The variability of GAN-produced samples is limited by that of the original set [29]; therefore, if few images contain extreme dilations, the generated images would too [29]. To the best of our knowledge, there are no available methods that address the DA of the pupil dilation level from existing images. The proposed approach aims to solve that by generating new examples of iris images of the same individual but under any desired dilation level. In this way, new datasets with a uniform distribution of dilation levels λ can be easily generated from readily available datasets.

III. ARTIFICIAL DILATION AUGMENTATION

The proposed method is a DA function that can change the dilation level λ_1 of an iris image, or semantically segmented mask, into any desired dilation level λ_2 . This function is based on traditional image processing and sampling methods, instead of deep learning, so it is fast and does not require any training.

In iris recognition, the coordinates of the circles that best fit the pupil and iris (Fig. 2c) are used to normalize the image, by means of polar coordinates. In this process, the annular region of the iris surface is transformed into a rectangle (Fig. 2d), known as rubber sheet, using (1) [4]. This normalization is not affected by dilation changes since the space between the pupil and iris is always normalized in the radial axis between 0 and 1 [4]. In other words, all of the iris images of a subject at any dilation level $\lambda_1, \lambda_2, \lambda_3, \dots, \lambda_n$ will be transformed into the same rubber sheet. Inspired by this normalization function, we sought an answer to the following question. Can the inverse of this transformation be used to synthesize an image with any desired dilation level λ_i from the rubber sheet?

$$I(x(r, \theta), y(r, \theta)) \rightarrow I(r, \theta) \quad (1)$$

By developing (1), we were able to derive the equation that can directly sample the coordinates of the image with dilation level λ_1 to produce a new image with dilation level λ_2 , without

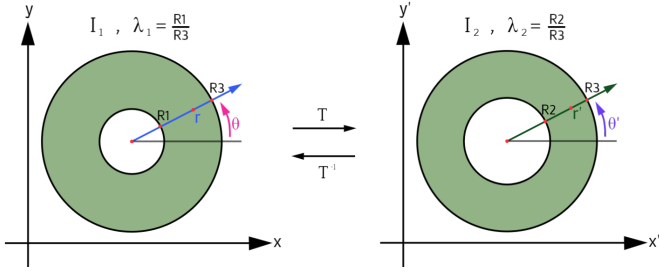


Fig. 3. Dilation Transformation Diagram.

even going to the normalized state. The resulting sampling equations can be best explained with the diagram of Fig. 3. Let I_1 and I_2 be two iris images at dilation states λ_1 and λ_2 respectively, R_1 and R_2 be the radius of the pupil iris boundary of these images, and R_3 be the radius of the iris sclera boundary in both images. The polar coordinates of a point in the iris surface of I_1 are represented by (r, θ) , and the coordinates of the corresponding point in I_2 are given by (r', θ') . The transformation $I_1 \rightarrow I_2$ is noted as T , and T^{-1} is the transformation $I_2 \rightarrow I_1$. Then, we can start to deduce the relationships between the coordinates of the two images.

We can first note that the angle is not going to be affected by this transformation. Otherwise, I_2 would be rotated. Therefore, we can conclude that, θ is the same as θ' . Then, only the radial component is going to be affected by the transformation. Since the normalization process is linear [4], we can conclude that, the distance between R_1 and r would be proportional to the distance between R_2 and r' as presented in (2).

$$\frac{r - R_1}{R_3 - R_1} = \frac{r' - R_2}{R_3 - R_2} \quad (2)$$

Then we can solve for r in order to know which point in I_1 must be sampled for a given r' in the output image I_2 (3).

$$r = \frac{R_3 - R_1}{R_3 - R_2}(r' - R_2) + R_1 \quad (3)$$

Equation (3) is valid for points in the iris surface; however, for the points inside the pupil, a slight variation, given in (4) and (5), must be used since they start when $r = 0$.

$$\frac{r - 0}{R_1 - 0} = \frac{r' - 0}{R_2 - 0} \quad (4)$$

$$r = \frac{R_1}{R_2}r' \quad (5)$$

For points outside the iris, r is the same as r' since points on the sclera and the skin are not affected by dilation. Equation (6) summarizes transformation T^{-1} for the entire image.

$$T^{-1} : \begin{cases} r_{r',\theta'} = (R_1/R_2)r' & , \text{ if } r' < R_2 \\ r_{r',\theta'} = m(r' - R_2) + R_1 & , \text{ if } R_2 \leq r' < R_3 \\ r_{r',\theta'} = r' & , \text{ if } R_3 \leq r' \\ \theta_{r',\theta'} = \theta' & , \text{ if } 0 \leq \theta' < 2\pi \end{cases} \quad (6)$$

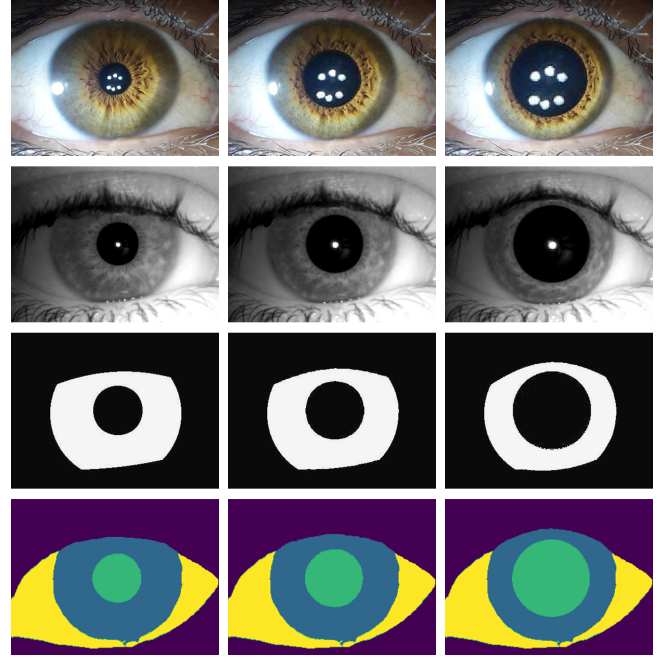


Fig. 4. Examples of artificially changing the dilation of a diversity of iris images using the proposed method. From top to bottom: Visible Light RGB image, Near Infrared Range grayscale image, binary mask, semantic mask with four classes.

In (6), the constant value m is equal to $(R_3 - R_1) \div (R_3 - R_2)$. Finally, the algebraic expressions in (7) can be used to transform from cartesian coordinates to polar coordinates, and thus T^{-1} can be used on the square grid of pixels of an image.

$$x = r \cos(\theta) \quad , \quad y = r \sin(\theta) \quad (7)$$

To synthesize image I_2 from I_1 , the intensity value of every pixel in I_2 comes from sampling the corresponding pixel in I_1 , whose coordinates are given by solving (6) and (7). Pixels are sampled with nearest-neighbor interpolation because it is the fastest sampling technique [30]. This approach is useful to reduce DA time while training semantic segmentation networks. However, other sampling techniques such as bilinear or bicubic can easily be implemented [30].

This method was applied for grayscale images, RGB images, binary segmentation masks, as well as multichannel semantic masks, as seen in Fig. 4. The only artifact is that eye leads that cross the iris are affected by T^{-1} , as if the subject opened their eyes. Nevertheless, the output images look very realistic, which is essential for network generalization.

The proposed method, implemented both in Python and Matlab, is publicly available on GitHub¹. It contains the raw DA functions, as well as didactic Graphical User Interface (GUI) examples.

¹<https://github.com/dpbenalcazar/ArtificialDilation>

IV. DATASETS

In this work we trained and tested several readily available semantic-segmentation networks using the datasets described in this section, in order to evaluate the performance of the proposed method. We selected two datasets, captured with the same capture device. These datasets were chosen to help testing the generalization capabilities of the networks in the presence of a wide range of pupil dilations.

For training and validation, we utilized the dataset captured by Benalcazar et al. [31], which tested iris recognition performance under two kinds of illumination. The commonly used NIR frontal illumination against frontal and lateral VL. This dataset consists of 96 subjects, five images of the right eye per subject, and 4 cases of illumination. There are 1,920 images in total, which were partitioned, in a person-disjoint manner, as 1,540 images for training and 380 for validation. The illumination conditions were controlled, so there is a small pupil dilation variation from image to image. The dilation distribution for the 1,920 images, seen in Fig. 5, has the following parameters: mean=0.347, STD=0.073, min=0.169, max=0.625.

For testing, we used the dataset that Benalcazar et al. [20] originally captured to train a network that predicts a 3D model of the iris tissue. For a better generalization, the authors captured a dataset with a wide range of pupil dilation. The subjects were exposed to darkness for 10 seconds, which dilated their pupils, then lights were turned on, and the contraction of the pupil was captured frame by frame for 3 seconds [20]. In that experiment, 26,520 images were captured; however, in this work, we utilized only a portion by uniformly sampling the dilation of each subject. Therefore, the test set in this work contains 120 subjects and ten images per eye of each subject, for a total of 2,400 images. The dilation distribution in this case, shown in Fig. 6, has the following parameters: mean=0.4, STD=0.112, min=0.158, max=0.711. It can be noted that both the standard deviation and the max dilation are greater in the test set; thus, learning meaningful features from the training set is very challenging. That is why the chosen datasets are perfect to evaluate the effects of the proposed DA method.

V. EXPERIMENTS

The purpose of our method is to help any iris semantic segmenter to perform better, specially under extreme dilation cases. In order to test the efficacy of our DA algorithm, we trained and tested seven readily available networks, with the previously described datasets, in two scenarios: Normal DA, and Artificial Dilation DA. Both scenarios were trained from scratch with the same hyper-parameters per network.

A. Data Augmentation Scenarios

Figure 7 illustrates the DA applied in the two scenarios. For Normal DA, the offline augmentation consisted of making 20 copies of the input images. Therefore, the networks were presented with 38,400 images each epoch. Then, during training, a random transformation of translation, scaling, flipping, brightness, and blurring was applied to each image.

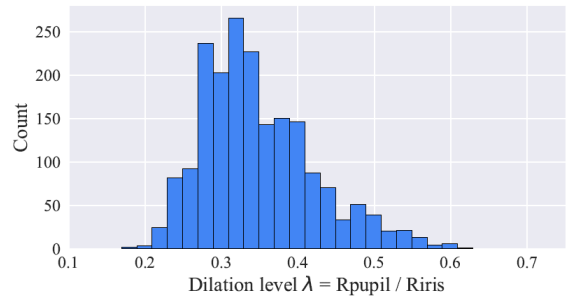


Fig. 5. Train Dataset Dilation Distribution

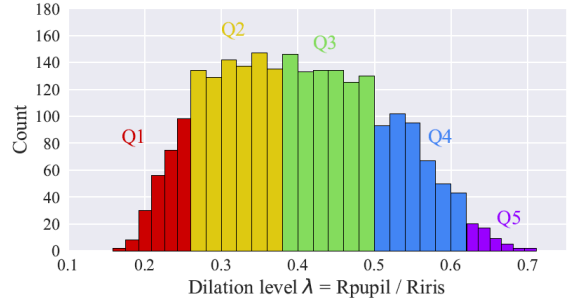


Fig. 6. Test Dataset Dilation Distribution by Quantiles

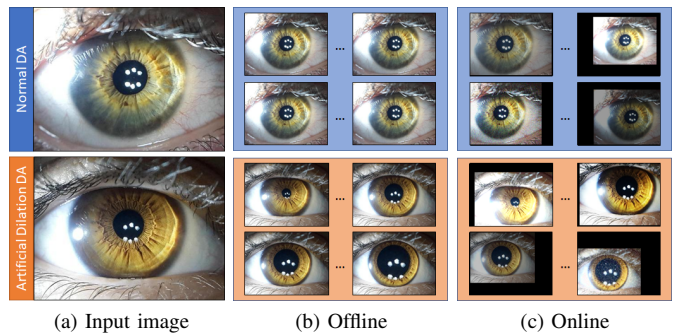


Fig. 7. DA schemes used in the experiments. a) Input image. b) Twenty offline augmentations. c) Random online DA during network training.

In Artificial Dilation DA, for each input image, we generated 19 artificial dilations using λ equally separated between 0.15 and 0.75. Adding the original input images, we also have 38,400 images each epoch. It is worth mentioning that we generated the augmented images offline for consistency purposes; however, the proposed method can be used online as well. After that, the same random transformations as Normal DA were applied online to each image while training the networks.

B. Trained Networks

The seven networks trained in this work are the following. CCNet [16], [23] and DenseNet10 [10], which were conceived for the purpose of iris semantic segmentation. They are based on the encoder-decoder architecture [10]. Using the same

TABLE I
MEAN IOU \pm STANDARD DEVIATION FOR THE ENTIRE TEST SET (2,400 IMAGES)

Augmentation	CCNet	DenseNet10	Vgg16-Unet	ResNet50-Unet	MobileNet2-Unet	pix2pix	CycleGAN
Normal	0.681 \pm 0.113	0.870 \pm 0.068	0.854 \pm 0.057	0.876 \pm 0.060	0.857 \pm 0.051	0.812 \pm 0.116	0.741 \pm 0.082
Artif. Dilation	0.722 \pm 0.141	0.879 \pm 0.057	0.875 \pm 0.058	0.880 \pm 0.053	0.880 \pm 0.050	0.894 \pm 0.055	0.750 \pm 0.089
Improvement	5.89%	1.07%	2.43%	0.45%	2.67%	10.09%	1.25%

TABLE II
PERCENTAGE OF MEAN IOU IMPROVEMENT FOR EACH QUANTILE OF THE TEST SET.

Quantile	Mean λ	CCNet	DenseNet10	Vgg16-Unet	ResNet50-Unet	MobileNet2-Unet	pix2pix	CycleGAN	Mean
Q1	0.2378	-0.33%	0.79%	1.61%	0.98%	1.49%	-0.02%	0.54%	0.72%
Q2	0.3250	2.97%	1.22%	2.01%	0.21%	2.33%	2.14%	0.35%	1.60%
Q3	0.4327	6.49%	0.72%	2.16%	0.26%	2.83%	9.91%	0.57%	3.28%
Q4	0.5361	12.30%	1.71%	3.40%	0.45%	3.43%	28.36%	2.54%	7.46%
Q5	0.6307	22.58%	0.30%	6.56%	2.08%	4.96%	56.80%	12.90%	15.17%

architecture, we employed three general purpose networks that have Unet [32] in the decoder, and VGG16 [33], ResNet50 [34] and MobileNet2 [35] in the encoder respectively. Finally, we trained pix2pix and CycleGAN [29], which are GANs that can translate the image to the semantic mask space. The semantic ground-truth masks used for training and testing have only two labels: iris and background.

In the hardware level, these networks require Graphics Processing Units (GPU) to accelerate training; however, during inference, they can produce results in a fraction of a second, even with single board computers such as the Raspberry Pi [23]. The networks were trained on a Ryzen5 machine with 16GB of RAM and a 12GB GPU.

C. Performance Metric

The metric that we use for performance evaluation is the bitwise Intersection over Union (IoU) [10]. This metric, described in (8), compares the ground truth and predicted segmentation masks (M_A and M_B) by counting the number of bits that are high in a logical AND operation between both masks, divided by the count of logical ones in the logical OR operation between them.

$$IoU = \frac{\sum(M_A \wedge M_B)}{\sum(M_A \vee M_B) + \epsilon} \quad (8)$$

This metric takes the range of values between 0 and 1, being 1 a perfect match. The constant ϵ has a small positive value that ensures the denominator never takes a value of zero.

VI. RESULTS

The results of the described experiments, evaluated on the 2,400 test images, are presented in Table I. This table shows the mean and STD values of the IoU metric, for each of the seven networks trained, with and without the proposed Artificial Dilation DA method. This table shows an increase in mean IoU value for all the trained models. The final row shows the relative improvement as a percentage. It can be seen that pix2pix and CCNet are the networks that improved the most with the proposed method. For instance, pix2pix increased mean IoU by 10.09% (from 0.812 to 0.894). On

the other side of the spectrum, DenseNet10 and ResNet50-Unet had a marginal improvement. This is because some networks have a richer architecture than others, thus, some can generalize well with normal DA, while others required the better examples provided by our method to learn. Overall, the average improvement produced by all the seven networks was 3.41%. The computed p-value for the T-test applied on Table I was 0.0394. This means that the increase in performance produced by our method was significant, with a probability of being caused by mere chance less than 5%. This implies that the proposed DA method is a meaningful tool to increase performance in iris semantic segmentation.

Table II shows the results divided by quantiles. This table analyzes the improvement margin when we divide the test set in five groups of equally separated dilation levels as depicted in Fig. 6. The column Mean λ shows the mean dilation level of each quantile. It can be seen that for Q1, Q2 and Q3, the improvement was less than 3.5%. However, mean IoU improved by 7.46% and 15.17% in Q4 and Q5 respectively. This indicates that our method has a greater impact in improving segmentation results on iris images with high dilation levels.

Additionally, we tested the speed of the python implementation. We augmented 100 NIR images of 320×280 pixels. The average time per image was 12.014, 2.725 and 2.696 ms on a Ryzen3, Ryzen5 and Intel Core-17 processors respectively. All machines had 16GB of RAM and used a single thread. The fastest time is equivalent to synthesizing 371 images per second, which is more than enough for real time training of a network.

VII. CONCLUSIONS

We developed a DA function that artificially changes the dilation level λ_1 of an iris image into any desired level λ_2 . This function enriches the dilation variability of any dataset, and can be applied both offline and online because of its speed. This method is based on sampling techniques, so it does not require any training. The proposed method improved the overall IoU in semantic segmentation networks by 3.41% in average, with a p-value of 0.0394. This means that our

method significantly increased the performance of the trained networks. We observed that the greatest improvement occurred in the quantile of highest dilation. In average, IoU increased by 15.17%. This means that the proposed DA method helps achieving better performance in iris segmentation tasks, specially for dilated images, which are scarce in most available datasets. This in turn would lead to a better iris recognition pipeline.

Future work includes implementing more robust sampling methods, such as bilinear, and improving the equations so they work over non-concentric elliptic segmentation. This would expand the potential of this method for working with in-the-wild datasets, which consist of a limited number of iris images from different perspectives.

ACKNOWLEDGMENT

This work was partially supported by TOC Biometrics R&D center SR-226, and SOVOS. Spacial thanks to the Department of Electrical Engineering, Universidad de Chile.

REFERENCES

- [1] K. Sundararajan and D. L. Woodard, "Deep learning for biometrics: A survey," *ACM Computing Surveys (CSUR)*, vol. 51, no. 3, pp. 1–34, 2018.
- [2] K. W. Bowyer, K. Hollingsworth, and P. J. Flynn, "Image understanding for iris biometrics: A survey," *Computer vision and image understanding*, vol. 110, no. 2, pp. 281–307, 2008.
- [3] M. S. Hosseini, B. N. Araabi, and H. Soltanian-Zadeh, "Pigment Melanin: Pattern for Iris Recognition," *IEEE Transactions on Instrumentation and Measurement*, vol. 59, no. 4, pp. 792–804, 2010.
- [4] J. Daugman, "How iris recognition works," in *The essential guide to image processing*. Elsevier, 2009, pp. 715–739.
- [5] K. W. Bowyer and M. J. Burge, *Handbook of iris recognition*. Springer, 2016.
- [6] J. Daugman, "600 million citizens of India are now enrolled with biometric ID," *SPIE newsroom*, vol. 7, 2014.
- [7] K. Hollingsworth, K. W. Bowyer, and P. J. Flynn, "Pupil dilation degrades iris biometric performance," *Computer Vision and Image Understanding*, vol. 113, no. 1, pp. 150–157, 2009.
- [8] S. S. Arora, M. Vatsa, R. Singh, and A. Jain, "Iris recognition under alcohol influence: A preliminary study," in *2012 5th IAPR International Conference on Biometrics (ICB)*. IEEE, 2012, pp. 336–341.
- [9] I. Tomeo-Reyes, A. Ross, and V. Chandran, "Investigating the impact of drug induced pupil dilation on automated iris recognition," *2016 IEEE 8th International Conference on Biometrics Theory, Applications and Systems, BTAS 2016*, 2016.
- [10] J. E. Tapia, E. L. Drogue, A. Valenzuela, D. P. Benalcazar, L. Causa, and C. Busch, "Semantic segmentation of periocular near-infra-red eye images under alcohol effects," *IEEE Access*, vol. 9, pp. 109 732–109 744, 2021.
- [11] A. Gangwar and A. Joshi, "Deepirisnet: Deep iris representation with applications in iris recognition and cross-sensor iris recognition," in *2016 IEEE international conference on image processing (ICIP)*. IEEE, 2016, pp. 2301–2305.
- [12] Z. Zhao and A. Kumar, "Towards more accurate iris recognition using deeply learned spatially corresponding features," in *Proceedings of the IEEE international conference on computer vision*, 2017, pp. 3809–3818.
- [13] K. Nguyen, C. Fookes, A. Ross, and S. Sridharan, "Iris recognition with off-the-shelf cnn features: A deep learning perspective," *IEEE Access*, vol. 6, pp. 18 848–18 855, 2017.
- [14] S. Minaee and A. Abdolrashidi, "Deepiris: Iris recognition using a deep learning approach," *arXiv preprint arXiv:1907.09380*, 2019.
- [15] T. Zhao, Y. Liu, G. Huo, and X. Zhu, "A deep learning iris recognition method based on capsule network architecture," *IEEE Access*, vol. 7, pp. 49 691–49 701, 2019.
- [16] S. Mishra, P. Liang, A. Czajka, D. Z. Chen, and X. S. Hu, "C-net: Image complexity guided network compression for biomedical image segmentation," in *2019 IEEE 16th International Symposium on Biomedical Imaging (ISBI 2019)*. IEEE, 2019, pp. 57–60.
- [17] Y.-H. Yiu, M. Aboulatta, T. Raiser, L. Ophay, V. L. Flanagan, P. Zu Eulenburg, and S.-A. Ahmadi, "Deepvog: Open-source pupil segmentation and gaze estimation in neuroscience using deep learning," *Journal of neuroscience methods*, vol. 324, p. 108307, 2019.
- [18] S. Lei, B. Dong, A. Shan, Y. Li, W. Zhang, and F. Xiao, "Attention meta-transfer learning approach for few-shot iris recognition," *Computers and Electrical Engineering*, vol. 99, p. 107848, 2022.
- [19] J. E. Zambrano, D. P. Benalcazar, C. A. Perez, and K. W. Bowyer, "Iris recognition using low-level cnn layers without training and single matching," *IEEE Access*, vol. 10, pp. 41 276–41 286, 2022.
- [20] D. P. Benalcazar, J. E. Zambrano, D. Bastias, C. A. Perez, and K. W. Bowyer, "A 3d iris scanner from a single image using convolutional neural networks," *IEEE Access*, vol. 8, pp. 98 584–98 599, 2020.
- [21] D. P. Benalcazar, D. A. Montecino, J. E. Zambrano, C. A. Perez, and K. W. Bowyer, "3d iris recognition using spin images," in *2020 IEEE International Joint Conference on Biometrics (IJCB)*. IEEE, 2020, pp. 1–8.
- [22] L. Omelina, J. Goga, J. Pavlovicova, M. Oravec, and B. Jansen, "A survey of iris datasets," *Image and Vision Computing*, vol. 108, p. 104109, 2021.
- [23] Z. Fang and A. Czajka, "Open source iris recognition hardware and software with presentation attack detection," in *2020 IEEE International Joint Conference on Biometrics (IJCB)*. IEEE, 2020, pp. 1–8.
- [24] I. Tomeo-Reyes, A. Ross, A. D. Clark, and V. Chandran, "A biomechanical approach to iris normalization," in *2015 International Conference on Biometrics (ICB)*. IEEE, may 2015, pp. 9–16. [Online]. Available: <http://ieeexplore.ieee.org/document/7139041/>
- [25] M. B. Lee, Y. H. Kim, and K. R. Park, "Conditional generative adversarial network-based data augmentation for enhancement of iris recognition accuracy," *IEEE Access*, vol. 7, pp. 122 134–122 152, 2019.
- [26] J. E. Tapia and C. Arellano, "Soft-biometrics encoding conditional gan for synthesis of nir periocular images," *Future Generation Computer Systems*, vol. 97, pp. 503–511, 2019.
- [27] J. Maureira, J. Tapia, C. Arellano, and C. Busch, "Synthetic periocular iris pai from a small set of near-infrared-images," *arXiv preprint arXiv:2107.12014*, 2021.
- [28] J. Maureira, J. E. Tapia, C. Arellano, and C. Busch, "Analysis of the synthetic periocular iris images for robust presentation attacks detection algorithms," *IET Biometrics*, 2022.
- [29] C. Chu, A. Zhmoginov, and M. Sandler, "Cyclegan, a master of steganography," *arXiv preprint arXiv:1712.02950*, 2017.
- [30] P. I. Corke and O. Khatib, *Robotics, vision and control: fundamental algorithms in MATLAB*. Springer, 2011, vol. 73.
- [31] D. Benalcazar, C. Perez, D. Bastias, and K. Bowyer, "Iris recognition: Comparing visible-light lateral and frontal illumination to nir frontal illumination," in *2019 IEEE Winter Conference on Applications of Computer Vision (WACV)*, 2019, pp. 867–876.
- [32] O. Ronneberger, P. Fischer, and T. Brox, "U-net: Convolutional networks for biomedical image segmentation," in *International Conference on Medical image computing and computer-assisted intervention*. Springer, 2015, pp. 234–241.
- [33] K. Simonyan and A. Zisserman, "Very deep convolutional networks for large-scale image recognition," *arXiv preprint arXiv:1409.1556*, 2014.
- [34] K. He, X. Zhang, S. Ren, and J. Sun, "Deep residual learning for image recognition," in *Proceedings of the IEEE conference on computer vision and pattern recognition*, 2016, pp. 770–778.
- [35] A. G. Howard, M. Zhu, B. Chen, D. Kalenichenko, W. Wang, T. Weyand, M. Andreetto, and H. Adam, "Mobilenets: Efficient convolutional neural networks for mobile vision applications," *arXiv preprint arXiv:1704.04861*, 2017.